LAWRENCE
LIVERMORE
NATIONAL
LABORATORY

UCRL-JRNL-211450

ULTRA-HIGH STRENGTH IN NANOCRYSTALLINE MATERIALS UNDER SHOCK LOADING

E. M. Bringa, A. Caro, Y. M. Wang, M. Victoria, J. McNaney, B. A. Remington, R. Smith, B. Torralva, H. Van Swygenhoven

April 18, 2005

Science

Ultra-high strength in nanocrystalline materials under shock loading

E.M. Bringa[1], A.J. Caro[1], Y.M. Wang[1], M. Victoria[1], J. McNaney[1], B.A. Remington[1], R. Smith[1], B. Torralva[1], and H. Van Swygenhoven[2]

[1]*Lawrence Livermore National Laboratory, Livermore, CA 94550, USA*

[2]*Paul Scherrer Institute,CH-5232,Villigen-PSI,Switzerland*

Molecular dynamics simulations of nanocrystalline (nc) copper under shock loading show an unexpected ultra-high strength behind the shock front. The strength at high pressure can be up to twice the value at low pressure, for all grain sizes studied here (5-50 nm grains, with up to ~4 10^8 atoms). Partial and perfect dislocations, twinning, and debris from dislocation interactions are found behind the shock front. Results are interpreted in terms of the pressure dependence of both deformation mechanisms active at these grain sizes, namely dislocation plasticity and grain boundary sliding. These simulations, together with new shock experiments on nc nickel, raise the possibility of achieving ultra-hard materials during and after shock loading.

Dislocations are the carriers of plastic deformation in crystalline materials (1). The search for materials with ultra-high hardness and strength is closely related to the search for the most effective obstacles to dislocation motion. Grain boundaries (GB) are effective obstacles for dislocation motions (1-3); the strength or hardness of crystalline materials increases inversely with the square root of their grain size - the Hall-Petch effect (2,3). Going to the nanoscale, however, this strengthening mechanism is limited by the onset of GB accommodation mechanisms, such as sliding (2-4). If such softening effects could be suppressed, even harder materials could be created, with potential applications to such extreme

environments, as target capsules for the National Ignition Facility (NIF) (5). We report in this paper results that show a substantial increase in strength during shock loading of nc Ni, with a complex dependence on shock pressure. The strength obtained right behind the shock front in the simulations is the largest ever observed for this model system.

Experimental observations of increased strength have been reported in high strain rate deformation of nanophase Ni and Cu, up to strain rates of 10^4/s (6-8). Dislocation plasticity in nanophase materials is controlled by thermal and mechanical activation of sources at GB's, a mechanism that requires fluctuations, implying an intrinsic time scale that could explain the reported strain rate sensitivity. Therefore, in the search of ultra-hard response to deformation one could imagine that by increasing the strain rate by several orders of magnitude, like in shock loading conditions (9,10), one would obtain an even harder material. However, extrapolation of strength from strain rates of 10^4/s to $>10^6$/s becomes problematic, because strain rate cannot be increased by orders of magnitude without incorporating an additional ingredient, namely, pressure. In fact when uniaxial loading is carried by a shock wave traveling faster than the sound velocity, lateral relaxation does not occur and pressure builds up. Under those conditions, a totally new regime is entered where plasticity is controlled by both high strain rate and high pressure. Here we present atomistic simulations of shocked nanocrystalline samples, where the extremely short compression time scales (or equivalently, very high volumetric strain rates) associated with shock loading are close to those observed in recent experiments (10-12). Such short time scales imply that dislocation creation and motion, and stress driven GB accommodation, are the dominant plasticity mechanisms; thermally activated processes are excluded. In what follows we present a qualitative model to describe the pressure dependence of the flow stress under these conditions.

Both GB accommodation and dislocation activity have a linear pressure dependence, although for different reasons. GB accommodation has similarities to the plasticity of granular media i.e. sliding of undeformable objects controlled by friction (13). In granular materials, the Mohr-Coulomb law of

sliding friction predicts that the onset of plasticity occurs when the applied stress is larger than the value defined by the flow stress, $\sigma_{flow} \propto (\sigma_0 + \alpha\sigma_{normal})$, where σ_0 is related to the cohesion of the interface, and α to the geometry of the grains. This criterion has been recently extended to nanocrystals (14,15). Associating σ_{normal} with pressure, we conclude that the onset threshold for sliding plasticity increases linearly with pressure (15). Using Molecular Dynamics (MD) simulations we have verified that a nc deforming plastically by GB accommodation gets harder as hydrostatic pressure is increased (16, Figs. S1, S2). With the scaling arguments presented in ref. (17) to express the grain size, d, dependence of deformation rate, the flow stress for GB sliding can tentatively be written as $\sigma_{GBS}=(\sigma_0 + \alpha P)(1+d/d_0)$, where σ_0 is the flow stress of a zero grain size material (an amorphous metal) at zero pressure, and d_o a constant. Note that σ_{GBS} increases as d increases in this regime. For shock-induced dislocation plasticity it is generally assumed that, as in the Steinberg-Guinan model (10), the dynamic strength/hardness of the material scales with the shear modulus, G, which in turn increases linearly with pressure, $G(P)=G_0+\beta P$ (10,16). Adding the Hall-Petch relation, the flow stress becomes $\sigma_{Disl}=C\ G(P)\ (d/d_1)^{-0.5}$, where C is assumed constant. The effective flow stress for a nanocrystal can be taken as $\sigma_{flow}=min(\sigma_{Disl},\sigma_{GBS})$, although a more realistic model would include a mixture of both when $\sigma_{Disl}\sim\sigma_{GBS}$. At any pressure, as grain size decreases, the material hardens according to Hall-Petch, down to the point where $\sigma_{Disl}=\sigma_{GBS}$, then for smaller grain sizes the material softens according to the law of GB sliding. As pressure increases, both mechanisms predict an increase in hardness creating the possibility for pressure-induced ultra-hard nanophase materials. Fig. 1 shows the qualitative hardness map that emerges from this model. These ultra-high hardness conditions can be achieved by shock loading (10-12).

In shock loading one surface of the system is driven inward along the z axis at a constant velocity U_p, leading to a shock wave with velocity U_s. The first major difference between homogeneous deformation (4,17-21), and shock loading (9), is that the total volumetric strain behind the shock front, ε, is constant

and determined by $\varepsilon = U_p/U_s$ ($d\varepsilon/dt$=0). (19) The stress along the shock direction behind the shock front, i.e. the shock "pressure", is also constant behind the front and given by $\sigma_{zz} = \rho_o U_p U_s$, where ρ_o is the density of the pre-shocked material. With U_p in the range 0.1-3.0 km/s, the shock pressure for copper is in the range ~5-230 GPa. Fig. 2 shows a typical shock profile. By increasing pressure, shear stress increases until the onset of plasticity occurs (peak in Fig. 2); then the flow stress decreases and evolves in a complex way depending on strain rate, pressure, microstructure, dislocation properties in the materials, etc; a satisfactory quantitative theory does not yet exist. The strain rate with which the material is deformed at the shock front is roughly given by ε divided by the shock front rise time, $d\varepsilon/dt \approx \varepsilon U_s/\Delta_z$, where Δ_z is the shock front width. This width depends on a number of factors, including grain size. Portions of the sample reached by the shock wave undergo a fast deformation, $d\varepsilon/dt \sim 10^9$-$10^{11}$/s, during the short shock rise time (~several ps) and then remain at constant strain, eventually relaxing the shear stress. Shock loading can irreversibly freeze-in some of the microstructural changes induced during the loading, producing a residual material still harder at zero pressure after the shock. Indeed, research over the last several decades shows clear indications of massive modification of the material after unloading and recovering of shocked materials (10-12,22).

We report large-scale MD shock simulations in Cu nanophase samples with up to ~4 10^8 atoms (16). Shock loading conditions are ideally modeled by large-scale MD simulations (9,23-26), which cover similar times and length scales as laser-shock experiments. Our simulations show for the first time that the large increase in shock pressure significantly reduces GB sliding, *i.e.* limits the softening mechanism, doubling the flow stress value. As a measure of σ_{normal} we use the trace of the stress tensor, *i.e.* the pressure. We measure the hardness/flow stress, via the von Mises stress (3), $\sigma_{flow}^2 = 0.5[(\sigma_{xx}-\sigma_{yy})^2+(\sigma_{yy}-\sigma_{zz})^2+(\sigma_{zz}-\sigma_{xx})^2]$. The main result of this work, the flow stress as a function of grain size and pressure, is shown in Fig. 3 (Fig. S3). At low stress (5 GPa), comparable to the stress of

quasi-static experiments, the hardness is low in relative terms; there is only GB sliding (4,18), and samples with small grains are softer than those with large grains. At intermediate stress (5–25 GPa) the hardness at all grain sizes increases with increasing shock strength. This is the manifestation of the reduction of GB sliding and harder dislocation plasticity, as discussed above. MD results in this pressure range are also shown in Fig. 1, showing qualitative agreement with our model. Fig. 3 confirms the predicted trends, including the shift in the position of the maximum hardness towards lower grain sizes as pressure increases. At large stress (>25 GPa), a new phenomenon appears, reflected in the drop in strength (σ_{flow}) shown in Fig. 3 (Fig. S3), as increased nucleation and motion of dislocations, together with a large increase in temperature allows the sample to deform more easily. At even higher pressures (150-220 GPa, depending on grain size) shock-induced melting occurs, with σ_{flow}~0, and therefore a maximum in hardness must exist at some intermediate pressure. We find the maximum hardness, about twice the value at "low" pressure, at ~25 GPa. For a simulation of realistic experimental conditions, this hardness increase is the largest ever observed for nc materials and may open new applications for nanomaterials, for instance in targets that will be shocked at NIF (5). The implications of our results for the design of these targets are twofold. First, given that spatial fluctuations in a shock front are of the order of the grain size, as seen in Fig. 2, using very small grains as target material would produce an extremely smooth shock front, as required to reach ignition in some designs. Second, the strength of nc materials could be beneficial for ignition designs that require a shell to hold over 0.7 GPa of DT gas fill.

To gain insight into the atomistic processes involved in the deformation we show in Fig. 4 a ~50 GPa shock wave traveling through 20 nm grains, where only defective atoms are shown (movie M1). We observe the traces of numerous stacking faults (sf) indicating the passage of partial dislocations. Our simulations also show nano-twins, represented by mirror planes. This is similar to atomistic simulations of homogeneous deformation (4,16-21) and shocks (9,4-26) at similar grain sizes. However, the most salient feature of this figure is the presence of perfect dislocations (Fig. S4), represented by narrow

ribbons of sf bounded by partial dislocations inside the grains. This phenomenon has not been observed before in quasi-static load simulations of Cu, which has low sf energy and also a low ratio of stable to unstable sf energies (21). Nano-twins have been reported for nc Al (20,27). The shock-induced nano-twin volume is less than 1% of the total volume at the end of our simulation. Twin growth is expected for longer pressure pulses, but experimental detection of this amount of twinning is difficult, given that a low density of twins already exists in the actual pre-shocked samples. We also find a number of defect clusters, about 1 nm in diameter, likely created by dislocation-dislocation interaction. These might act as dislocation obstacles as further deformation is carried out, contributing to increased hardness.

Shock-induced dislocation nucleation has been observed in numerous studies, but a detailed understanding has begun to emerge only recently. The barriers for dislocation nucleation do not increase strongly with pressure (28) above an initial threshold, at least in the shock regimes studied here for fcc Cu. Studies of shock waves in single crystal Cu with and without defects (9,24-26) show increased dislocation production with shock pressure, *i.e*. pressure does not inhibit the nucleation process. We find the same behavior for nc at all grain sizes, with a threshold of ~6 GPa, even for 5 nm grains (Fig. S5). As pressure increases, dislocations nucleate initially at GB junctions (movie M2), and then from different locations along the GB. The fact that the stress is high enough to induce dislocation creation at such small grain size is due to the reduction of GB sliding, a mechanism that, if dominant, would release the shear stress. This behavior can further be understood in terms of the differences in the pressure dependence of both GB sliding and the dislocation nucleation processes, which decreases the grain size at which the maximum hardness occurs as pressure increases, as shown in Figs. 1 and 3.

In addition to the simulations shown here, we are performing experiments as part of our effort to understand the behavior of nc metals under extreme conditions. Due to experimental constraints, it is extremely difficult to directly measure the dynamic deformation process during high-strain rate loading at the nano-scale and there are no reported experiments on nc metals above 10^4/s. For the first time, we

have successfully carried out high-pressure, high strain rate loading and recovery (12) of a nc metal (29). Fig. 5 shows a plan-view transmission electron microscopy picture of nc Ni after shock loading at 40 GPa (16). Ni and Cu are both fcc materials with very similar shock impedances, but Ni has larger sf energy. There is clear evidence of dislocation activity occurring inside grains (boxes in Fig. 5) (29) in agreement with our atomistic simulations. During loading at ~40 GPa, our MD simulations predict a dislocation density of ~10^{13}/cm^2, which is expected to decrease during recovery. Although the exact dislocation density in recovered samples is difficult to estimate, our TEM and HRTEM images do show residual dislocations inside multiple nano-grains (Fig. 5). This is quite unusual in nc materials and not achievable under normal deformation conditions (30). Fig. 3 shows an increase in hardness *during shock loading*. Our experiments also show an increase in hardness in the samples recovered *after shock loading*, as expected from the measured residual dislocation densities.

In summary, computer simulations of shocks in nc Cu show that the flow stress reaches ultra-high values at high pressure due to shock loading. This hardness increase, of up to a factor of two compared to un-shocked samples, arises because the barriers for GB sliding increase with pressure (13-15), while dislocation nucleation is not as sensitive to pressure above a threshold of several GPa. Although the simulations we have carried out are for nc Cu, GB sliding reduction under pressure should be a general feature of shock-loaded materials, including nc alloys and non-metallic nanocrystals. Harder nc-materials could offer novel applications, including improved armor materials and National Ignition Facility targets (5). Extensive experiments on shock loading and recovery of nc samples are in progress and should provide new insights into the behavior of nanophase materials at extreme conditions.

References and Notes

1. R. Madec, B. Devincre, L. Kubin, T. Hoc, and D. Rodney, Science **301**, 1879 (2003).

2. M.A. Meyers and K.K. Chawla, *Mechanical Behavior of Materials*, Prentice Hall, (1998).

3. J. R. Weertman, in *Nanostructured Materials: Processing Properties and Potential Applications*, C.C.

Koch, Ed. (William Andrew, Norwich, NY, 2001).

4. J. Schiøtz and K.W. Jacobsen, Science **301**, 1357 (2003).

5. T.R. Dittrich *et al*., Laser and Particle Beams **17**, 217 (1999).

6. D. Jia, K.T. Ramesh, E. Ma, L. Lu and K. Lu, Scripta Mater. **45**, 613 (2001).

7. L. Lu, S.X. Li and K. Lu, Scripta Mater. **45**, 1163 (2001).

8. F. Dalla Torre *et al.*, Acta Mater. **50**, 3957 (2002).

9. L. Holian and P.S. Lomdahl, Science **280**, 2085 (1998).

10. B. Remington *et. al*., Met. Mat. Trans. A **35**, 2587 (2004).

11. M. Meyers *et al.*, Act. Mater. **51** 1211 (2003).

12. J. M. McNaney, J. Edwards, R. Becker, T. Lorenz, B. Remington, Met. Trans A **35A**, 2625 (2004).

13. C.A. Schuh and A.C. Lund, Nature Materials **2**, 449 (2003).

14. A.C. Lund and C.A. Schuh, Acta Mater. **53**, 3193 (2005).

15. B. Jiang and G.J. Weng, J. Mech. Phys. Solids **52**, 25 (2004).

16. Modeling and experimental details are available as supporting material on *Science* Online.

17. H. Van Swygenhoven and A. Caro, Phys. Rev. **B 58**, 11246 (1998).

18. H. Van Swygenhoven, M. Spaczer, A. Caro, and D. Farkas. Phys. Rev. **B 60**, 22 (1999).

19. J. Schiøtz, F.D. Di Tolla, K.W. Jacobsen, Nature **391**, 561 (1998).

20. V. Yamakov *et al*., Nature Materials **1**, 1 (2002).

21. H. Van Swygenhoven, P. M. Derlet, and A.G. Frøseth, Nature Materials **3**, 399 (2004).

22. M.W. Chen, J. W. McCauley, and K. J. Hemker, *Science* 299, 1563 (2003).

23. K. Kadau, T. C. Germann, P.S. Lomdahl, B.L. Holian, Science **296**, 1681 (2002).

24. E. Bringa *et al*, J. App. Phys. **96**, 3793 (2004).

25. F. A. Sapozhnikov, V.V. Dremov and M.S. Smirnova, J. Phys. IV France **110**, 323 (2003).

26. L. Davila *et al*., Appl. Phys. Lett. **86**, 161902 (2005).

27. M.W. Chen, E. Ma, K.J. Hemker, H.W. Sheng, Y.M. Wang, X. Cheng, Science **300**, 1275 (2003).

28. S. Cheng, J.A. Spencer, and W.W. Milligan, Act. Mater. **51**, 4505 (2003).

29. Y.M. Wang *et al*., in preparation.

30. Z. Budrovic, H. Van Swygenhoven, P.M. Derlet, S. Van Petegem, and B. Schmitt., Science **304**, 273 (2004).

31. Authors would like to thank A. Hodge and C. Schuh for help with the experiments and valuable comments, D. Farkas for useful discussions and help running LAMMPS, P. Erhart for calculating the pressure dependent elastic constants, T. Diaz de la Rubia, R. Lebensohn, M.A. Meyers, V. Bulatov, N. Park and V. Dremov for useful discussions, and M. Duchaineau for help plotting the results. The work was performed under the auspices of the U.S. Department of Energy by University of California, Lawrence Livermore National Laboratory under contract No. W-7405-Eng-48, LDRD 04-ERD-021.

Supporting Online Material: www.sciencemag.org, Simulation details, Experimental Methods, Figs. S1-S5, Movies M1, M2.

Figure captions

Fig. 1: Flow stress for different pressures, as a function of grain size, according to our qualitative model (16). MD results are also included. In this plot we use parameters from the literature or calculated using our MD simulations (16): σ_0=0.9 GPa, α=0.04, β=1.0; G_0=45 GPa. We choose d_0=d_1=30 nm, and request that $\sigma_{Disl}(d_0)=\sigma_{GBS}(d_0)$ at P=0 GPa, to obtain C, the only free parameter left, C=0.04.

Fig. 2: Typical stress profiles under uniaxial shock loading: σ_{zz} ("shock pressure") and twice the flow stress. Values obtained from a snapshot of our MD simulation (d~20 nm), ~10 ps after the "piston" began to move with velocity U_p, advancing from left to right. The material has a "flow" velocity, U_{flow}=U_p=1 km/s, giving U_s=5.5 km/s, and ε_v~20% behind the shock front. The shock front spreads more than in single crystal simulations (8), with a width close to the grain size.

Fig. 3: Flow stress under shock loading at different shock wave pressures (σ_{zz}). The flow stress is largest in the range 20-30 GPa. Total volumetric strains behind the shock front are also indicated. The flow stress was averaged over ~20 nm, in a region in front of the piston, when the shock front had already traveled ~100 nm, as shown in Fig. 2.

Fig. 4: Snapshot of our simulation for d=20 nm and σ_{zz}=47 GPa (only a thin slab, 0.7 nm wide, is shown). The shock has traveled 30 ps, from bottom to top, producing a high density of partial dislocations (attached to GB's) together with perfect dislocations ('isolated' inside grains, Fig. S4) and nano-twins.

Fig. 5: A plan-view transmission electron microscopy image of nanocrystalline Ni after shock loading at 40 GPa. Dislocation activity is visible inside grains (white boxes), and the inset shows a filtered image of the dislocation. The grain sizes before the shock-loading are 30-50 nm. The final grain sizes are in the range 5-100 nm due to the residual shock heating in the recovered sample (29).

Figures

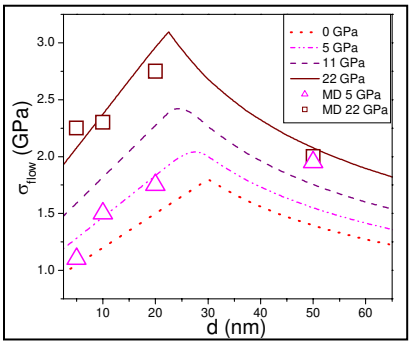

Fig. 1: Flow stress for different pressures, as a function of grain size, according to our qualitative model (16). MD results are also included. In this plot we use parameters from the literature or calculated using our MD simulations (16): σ_0=0.9 GPa, α=0.04, β=1.0; G_0=45 GPa. We choose d_0=d_1=30 nm, and request that $\sigma_{Disl}(d_0)=\sigma_{GBS}(d_0)$ at P=0 GPa, to obtain C, the only free parameter left, C=0.04.

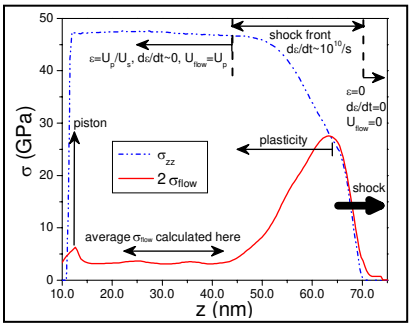

Fig. 2: Typical stress profiles under uniaxial shock loading: σ_{zz} ("shock pressure") and twice the flow stress. Values obtained from a snapshot of our MD simulation (d~20 nm), ~10 ps after the "piston" began to move with velocity U_p, advancing from left to right. The material has a "flow" velocity, U_{flow}=U_p=1 km/s, giving U_s=5.5 km/s, and ε_v~20% behind the shock front. The shock front spreads more than in single crystal simulations (8), with a width close to the grain size.

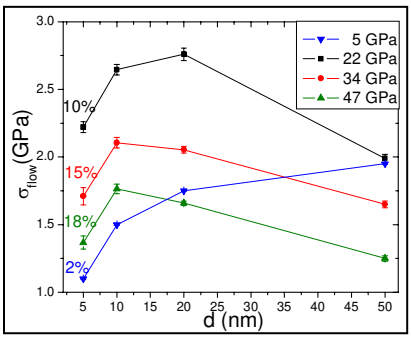

Fig. 3: Flow stress under shock loading at different shock wave pressures (σ_{zz}). The flow stress is largest in the range 20-30 GPa. Total volumetric strains behind the shock front are also indicated. The flow stress was averaged over ~20 nm, in a region in front of the piston, when the shock front had already traveled ~100 nm, as shown in Fig. 2.

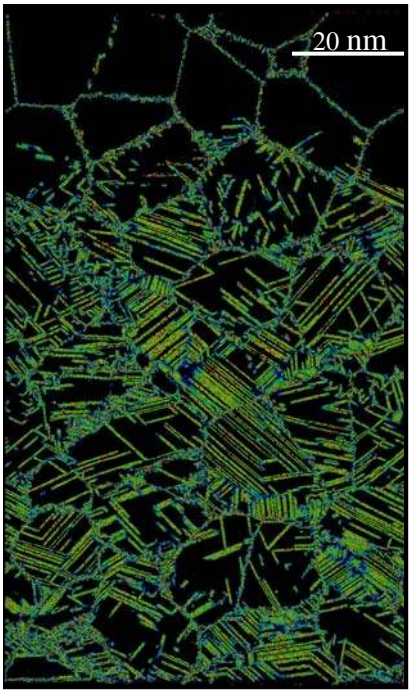

Fig. 4: Snapshot of our simulation for d=20 nm and σ_{zz}=47 GPa (only a thin slab, 0.7 nm wide, is shown). The shock has traveled 30 ps, from bottom to top, producing a high density of partial dislocations (attached to GB's) together with perfect dislocations ('isolated' inside grains, Fig. S4) and nano-twins.

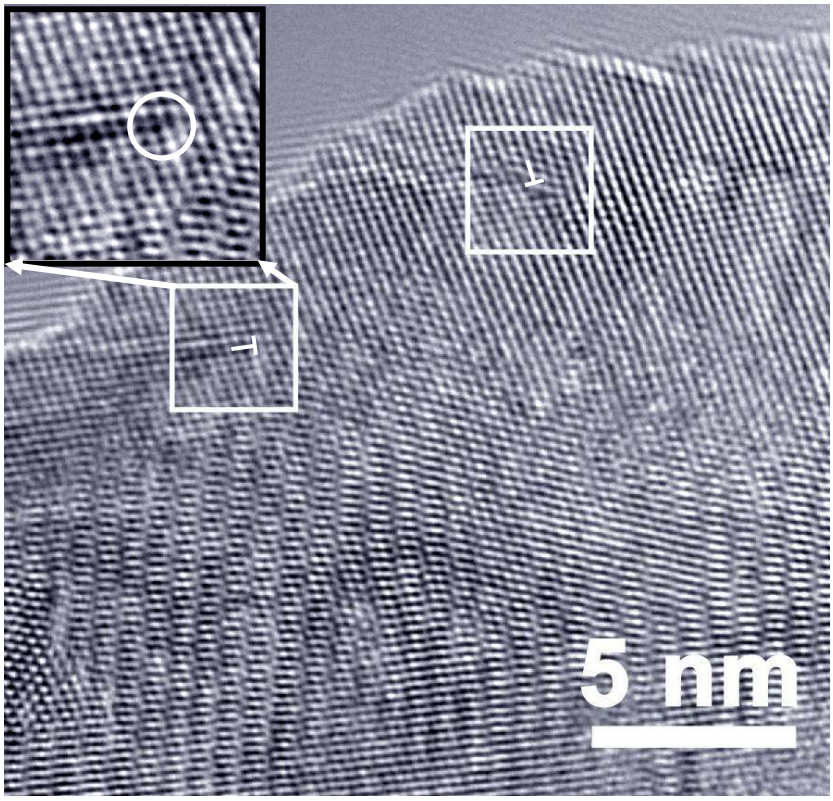

Fig. 5: A plan-view transmission electron microscopy image of nanocrystalline Ni after shock loading at 40 GPa. Dislocation activity is visible inside grains (white boxes), and the inset shows a filtered image of the dislocation. The grain sizes before the shock-loading are 30-50 nm. The final grain sizes are in the range 5-100 nm due to the residual shock heating in the recovered sample (29).

Supporting Online Material

Analytical flow stress model parameters

The model gives the flow stress as: $\sigma_{flow}=min(\sigma_{Disl},\sigma_{GBS})$, with $\sigma_{GBS}=(\sigma_0+\alpha P)(1+d/d_0)$ due to grain boundary (GB) sliding and $\sigma_{Disl}=C\,(G_0+\beta P)\,(d/d_1)^{-0.5}$ due to dislocation activity. σ_0 is the flow stress of a zero grain size material (an amorphous metal) at zero pressure and has been estimated to be 0.9 GPa (1). α gives the pressure dependence of GBS and has been given as 0.03-1.3, from energy minimization calculations of deformation in amorphous metals (2). It is likely strain rate dependent. We use α=0.04 to compare to our results. A larger value would shift the maximum hardness towards smaller grain sizes. Using molecular dynamics (see *Simulation Details* below) we have calculated the elastic constants as a function of pressure (at T=0 K) to obtain the shear modulus as $G(P)=G_0+\beta P$, with G_0=45 GPa and β~1 for P<60 GPa, in agreement with experiments (3). The Steinberg-Guinan model (4) gives only negligible temperature dependence for G for Cu and Ni. The only free parameters left are d_0, d_1, and C. Assuming the maximum hardness happens for P=0 at $d_0=d_1$, C can be determined by setting $\sigma_{Disl}(d_0)=\sigma_{GBS}(d_0)$. From simulations and experiments it is generally found that d_0=10-50 nm (5). Choosing d_0=30 nm we obtain C=0.04 and find good agreement between the predictions of the model and our simulation data. We note that most of the large body of research on ultra-high strain rate deformation typically neglects any effects due to GB, including GB accommodation/sliding. Our simple model accounts for this, neglecting possible temperature and strain rate effects that could be added to gain quantitative accuracy.

Simulation Details

Molecular-dynamics (MD) simulations describe a large collection of atoms, evolving in time due to inter-atomic forces derived from empirical potentials and offer details at the sub-nm scale not accessible with continuum models. Simulations were run on the Multi-programmatic Capability Resource (MCR) and Thunder Linux clusters at Lawrence Livermore National Laboratory, using from 64 to 4000 CPU's.

The embedded atom method (EAM) potential for Cu due to Mishin *et al.* (6) was used. This potential has been fitted to experimental lattice parameter (a_o=0.3615 nm), stacking fault (sf) energy and ab-initio P-V curve, among other parameters. Interactions include up to 4th nearest neighbors (54 atoms) at the equilibrium density. This potential gives a sf energy of 45 mJ/m^2 and the ratio of unstable to stable stacking fault energy is ~0.3, making difficult the emission of a second, trailing partial after a leading partial is emitted (7). Our nanocrystalline samples were built using the Voronoi polyhedra construction, with a density equal to 99% of the perfect crystal value, and including both high and low angle GB's in a random selection of grain orientations (8). Partial dislocation cores were identified using a centro-symmetry parameter (CSP) filter (9).

For a fluid, the von Mises stress would be zero; for a solid instead, it is larger than zero and changes with pressure. In most quasi-static simulations, for homogeneous deformation along z, $\sigma_{xx} = \sigma_{yy}$=0, then $\sigma_{VM} = \sigma_{zz}$. For simulations at constant strain rate, as in Fig. S1, the flow stress is typically measured at a fixed strain [e.g., 7-10% in ref. (5)]. For simulations at constant stress (7,8), the flow stress is measured at a given strain rate. In the shock wave simulations, the value of the von Mises stress corresponds to a fixed total strain and fixed strain rate, which are a function of the shock wave pressure. Stress, as shown in Fig. 2, was calculated in slices of width a_o perpendicular to the shock direction.

Homogeneous deformation simulations: We have carried out MD simulations of homogeneous uniaxial compression (5,7,8) at strain rates similar to those in shock-loading (10), and much higher than those used before (5,7,8), using LAMMPS (11). Homogeneous deformation at these strain rates, typical of shock loading, cannot be attained experimentally. Fig. S1 shows stress-strain curves for a 5 nm grain size Cu sample, at two different pressures, *P*: *P=0* GPa and *P~15* GPa. The relaxed nc sample, initially at *P=0* GPa, was compressed up to the desired hydrostatic pressure, relaxed at that pressure, and then deformed along the *z* axis while keeping $\sigma_{\perp}=\sigma_{xx} = \sigma_{yy}=P$. An ideal material without plastic deformation would display the linear elastic behavior shown in Fig. S1, but plasticity causes a departure from this

behavior. Since there are no dislocations, as discussed next, plasticity must be due to GB accommodation. Previous simulations at *P=0* GPa at this grain size (5,7,8) suggested that plastic deformation essentially occurs by GB sliding, with little or no dislocation activity. This is confirmed by our simulations, including the pressurized case, as shown in Fig. S2: there are no dislocations at 6.7% deformation. As assumed in our analytical model (Fig. 1), as pressure increases, the flow stress increases, indicating a substantial reduction of GB sliding, even though the strain rate is the same in both cases.

Shock simulations: The shock simulations were run using MDCASK (12). Our samples were tetragonal with free surfaces along the shock direction and periodic boundary conditions (PBC) in the transverse directions. They were equilibrated at 5-50 K for several ps before applying the shock. The first nm on one side was chosen as a piston and atoms there were moved at the desired piston velocity, U_p (10). Shocked samples were at least ~5x5x10 d^3, giving more than 250 grains/sample, except for the 50 nm sample, of ~3x3x4 d^3 (60 grains). To minimize fluctuations in the comparison of results due to possibly different grain boundary structure, the same set of grain location and orientations was used for all grain sizes studied. For *d*=5 nm a second sample was prepared with a rectangular cross section leading to a different grain distribution. The resulting stresses at a few pressures were the same within our error bars.

Fig S4 shows a 3-dimensional view of a region of a 20 nm sample after the passage of a ~50 GPa shock. There are perfect dislocations together with partial dislocations that leave behind a sf. Fig. S5 shows several snapshots of a 5 nm grain size sample loaded at different pressures, where significant dislocation activity can be seen.

Experimental methods

Experimental details will be published in a separate paper (13). Here only a brief summary is given. Goodfellow electrodeposited nc Ni foils were used (nominal size 15 nm, 300 μm thickness). The Philips CM-300 FEG TEM at LLNL was used in this study. TEM of the "as-received" foils gave grain sizes in

the range 30-50 nm. Foils were glued to a polycrystalline Cu substrate and loaded at room temperature at high strain rate at the Omega laser, as described elsewhere (14,15), giving a load rise time of few ns and peak pressures in the range 20-40 GPa. The wave steepens into a shock wave with a rise time of few ps after traveling 25-100 μm into the sample. The residual shock temperature for a 40 GPa shock has been estimated to be ~400-550 K, lasting several μs. As indicated in Fig. 5, this could result in modification of grain sizes and lower dislocation densities after recovery. Recovered samples were prepared for TEM analysis, resulting in Fig. 5.

References

1. Y. Estrin *et al*., J. Metastable Nanocrystalline Mat. **17**, 29 (2003).

2. C.A. Schuh and A.C. Lund, Nature Materials **2**, 449 (2003).

3. *Landolt-Börnstein New Series Tables*, Springer-Verlag (1986).

4. D. J. Steinberg, *Equation of State and Strength Properties of Selected Materials*, Lawrence Livermore National Laboratory report, UCRL-MA-106439 (1991).

5. J. Schiøtz and K.W. Jacobsen, Science **301**, 1357 (2003).

6. Y. Mishin, M. J. Mehl, D. A. Papaconstantopoulos, A. F. Voter, and J. D. Kress, Phys. Rev. B **63**, 24106 (2001).

7. H. Van Swygenhoven, P. M. Derlet, and A.G. Frøseth, Nature Materials **3**, 399 (2004).

8. H. Van Swygenhoven, M. Spaczer, A. Caro, and D. Farkas. Phys. Rev. **B 60**, 22 (1999).

9. C.L. Kelchner, S.J. Plimpton, and J.C. Hamilton, PRB **58**, 11085 (1998).

10. E.M. Bringa *et al*., J. App. Phys. **96**, 3793 (2004).

11. S. J. Plimpton, J. Comp. Phys. **117**, 1 (1995). http://www.cs.sandia.gov/~sjplimp/lammps.html

12. MDCASK: http://www.llnl.gov/asci/purple/benchmarks/limited/mdcask/

13.Y.M. Wang *et al*., in preparation.

14. J. Edwards *et al*., Phys. Rev. Lett. **92**, 075002 (2004).

15. J. M. McNaney, J. Edwards, R. Becker, T. Lorenz, B. Remington, Met. Trans A **35A**, 2625 (2004).

Supplementary Figures

Fig. S1: Simulated uniaxial compression curves for different initial pressures, at 1.3 10^{11}/s. The ideal elastic behavior (σ=$Y\varepsilon$, with Y the Young modulus) is also shown at both pressures. The starting sample is a relaxed nc Cu cube, 5 nm grain size, with a side of ~20 nm. T=300 K and $\sigma_{\perp}$ =0-15 GPa (σ_{zz}= σ_{VM} - $\sigma_{\perp}$).

Fig. S2. Microstructure corresponding to Fig. S1, showing the absence of dislocations inside grains even after large deformation. (A) Undeformed sample, (B) 6.7% deformation, $\sigma_{\perp}$=0 GPa; and (C) 6.7% deformation, $\sigma_{\perp}$=14.75 GPa.

Fig. S3: Flow stress under shock loading at different strains, for different grain sizes. The strain is uniquely related to a given pressure, and some pressures are indicated in the figure.

Fig. S4: Same sample as in Fig. 4, showing: a) perfect dislocations (highlighted by black arrows): leading and trailing partial dislocations with a narrow sf ribbon, and b) partial dislocation loops (white arrows) that leave behind a stacking fault represented by a couple of neighboring red planes still attached to the grain boundary. Centro-symmetry parameter (9) coloring.

Fig. S5: Thin slabs from snapshots of our simulations for a grain size d=5 nm and σ_{zz} =5 (A), 22 (B), 35 (C) and 47 (D) GPa, showing significant dislocation activity increasing with shock pressure.

Supplementary Movies

Movie M1 (mpg, 2.5 MB). 47 GPa shock for a nc with d=20 nm. Only a slice with defective atoms is shown.

Movie M2 (avi, 3.0 MB). 22 GPa shock for a nc with d=5 nm. Only a slice with defective atoms is shown.

Supplementary Figures

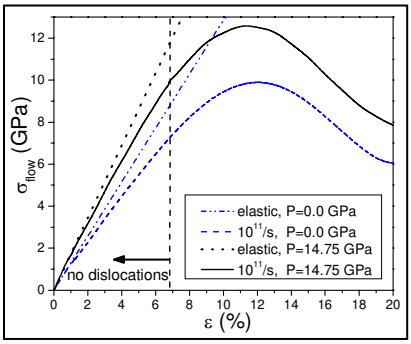

Fig. S1: Simulated uniaxial compression curves for different initial pressures, at 1.3 10^{11}/s. The ideal elastic behavior (σ=$Y\varepsilon$, with Y the Young modulus) is also shown at both pressures. The starting sample is a relaxed nc Cu cube, 5 nm grain size, with a side of ~20 nm. T=300 K and $\sigma_{\perp}$ =0-15 GPa (σ_{zz}= σ_{VM} - $\sigma_{\perp}$).

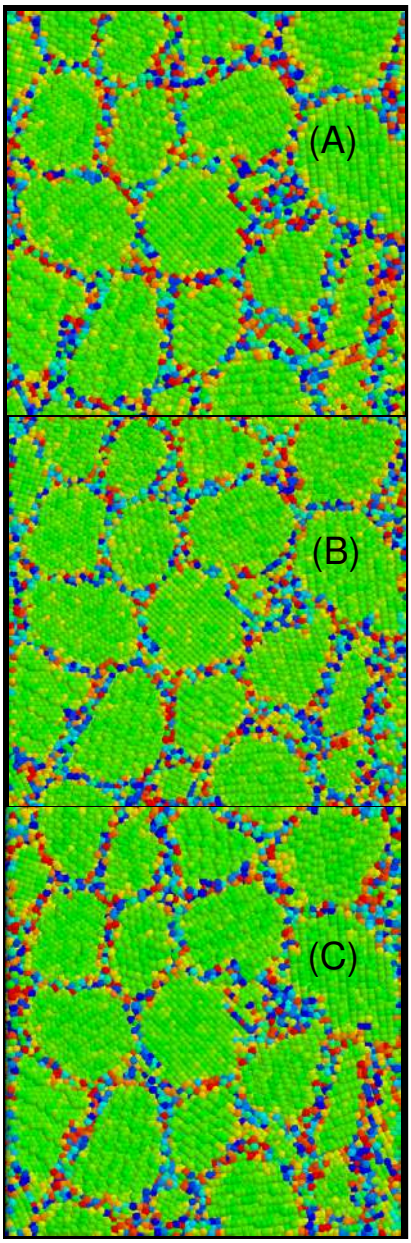

Fig. S2. Microstructure corresponding to Fig. S1, showing the absence of dislocations inside grains even after large deformation. (A) Undeformed sample, (B) 6.7% deformation, $\sigma_{\perp}$=0 GPa; and (C) 6.7% deformation, $\sigma_{\perp}$=14.75 GPa.

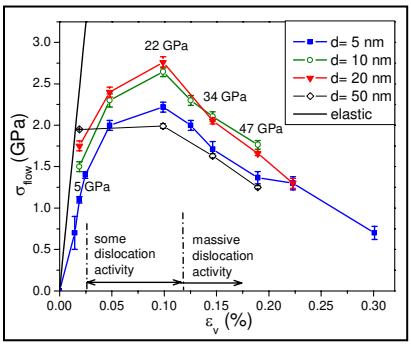

Fig. S3: Flow stress under shock loading at different strains, for different grain sizes. The strain is uniquely related to a given pressure, and some pressures are indicated in the figure.

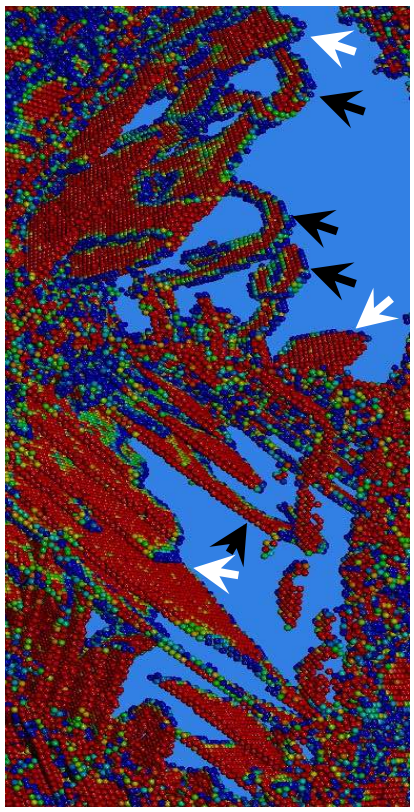

Fig. S4: Same sample as in Fig. 4, showing: a) perfect dislocations (highlighted by black arrows): leading and trailing partial dislocations with a narrow sf ribbon, and b) partial dislocation loops (white arrows) that leave behind a stacking fault represented by a couple of neighboring red planes still attached to the grain boundary. Centro-symmetry parameter (9) coloring.

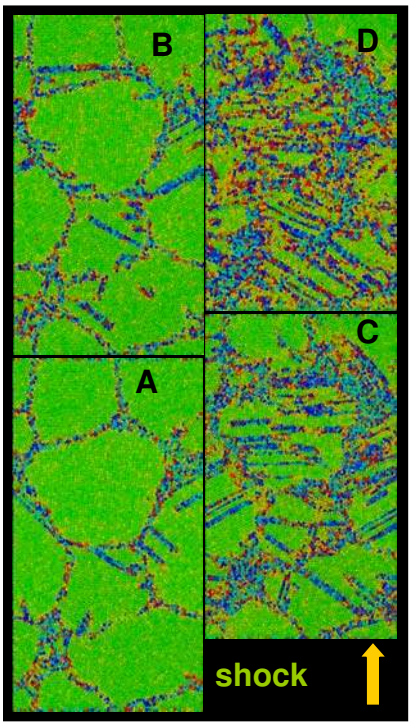

Fig. S5: Thin slabs from snapshots of our simulations for a grain size d=5 nm and σ_{zz} =5 (A), 22 (B), 35 (C) and 47 (D) GPa, showing significant dislocation activity increasing with shock pressure.